PHYSICAL REVIEW B **82**, 201402(R) (2010)

Nonlinear optical response of graphene in time domain

Kenichi L. Ishikawa*
Photon Science Center, Graduate School of Engineering, The University of Tokyo, 7-3-1 Hongo, Bunkyo-ku, Tokyo 113-8656, Japan
(Received 21 October 2010; published 4 November 2010)

We study nonlinear optical response of electron dynamics in graphene to an intense light pulse within the model of massless Dirac fermions. The time-dependent Dirac equation can be cast into a physically transparent form of extended optical Bloch equations that consistently describe the coupling of light-field-induced intraband dynamics and interband transitions. We show that the nonlinear optical response is not sufficiently described neither by pure intraband nor by pure interband dynamics but their interplay has to be taken into account. When the component of the instantaneous momentum parallel to the field changes its sign, the interband transition is strongly enhanced and considerably influences the intraband dynamics. This counteracts anharmonic response expected from purely intraband dynamics and relaxes nonlinearly. Nevertheless, graphene is still expected to exhibit nonlinear optical response in the terahertz regime such as harmonic generation.

DOI: 10.1103/PhysRevB.82.201402 PACS number(s): 78.67.Wj, 42.50.Hz, 42.65.Ky, 73.50.Fq

Despite its short history after the first intentional production,[1] there is rising interest in graphene over a wide spectrum of fields including materials, condensed-matter, optical, high-field, and high-energy science because of their potential application in carbon-based electronics as well as possibility to mimic and test quantum relativistic phenomena.[2,3] While unique properties such as finite conductivity at zero carrier concentration[4] and ac and dc universal conductance[5–7] are predicted and observed, the interest in the optical response of graphene is even further boosted by recent progress of terahertz (THz) radiation technology, which is another frontier research area.[8] The generation of ultrashort (from a few cycles even down to a single cycle) high-intensity [>100 MV/cm at 30 THz (Ref. 9) and 70 kV/cm at 1 THz (Ref. 10)] pulses has been reported, and even THz generation is possible from laser-irradiated graphite.[11] This will open up a new field of high-field physics in condensed matter. Along these lines the nonlinear optical response of graphene, such as induced current nonlinear in field strength and harmonic emission is becoming one of the key issues.[12–18] Using a quasiclassical kinetic approach but ignoring interband transitions, Mikhailov and Ziegler[12] predicted strong nonlinear response while Wright *et al.*[13] have performed Fourier analysis of the time-dependent Dirac equation (TDDE).

In this Rapid Communication, we study the time-domain nonlinear dynamics of the electric current induced in graphene by an ultrashort intense optical field, starting from the (2+1)-dimensional TDDE for massless fermions. Special emphasis is placed on the interplay between intraband and interband dynamics, which we describe with a set of extended optical Bloch equations (EBOEs) derived from the TDDE. The analysis using our model indicates that the induced current is dominated by the intraband dynamics but significantly affected by interband transitions. The underlying mechanism is that the latter is strongly enhanced when the instantaneous kinetic momentum of the electron passes near the Dirac point. This results in reduction in nonlinearity.

Let us first study the response of a single electron in graphene under an in-plane applied field $E(t)$ polarized along the x axis. To this end, we begin with the TDDE for the two-component wave function ψ,

$$i\hbar\frac{\partial}{\partial t}\psi = v_F\begin{pmatrix} 0 & pe^{-i\phi}+eA(t) \\ pe^{i\phi}+eA(t) & 0 \end{pmatrix}\psi, \tag{1}$$

where $v_F \approx c/300$, p denotes the magnitude of the canonical momentum $\mathbf{p}=(p_x,p_y)$, ϕ the directional angle satisfying $p_x=p\cos\phi$ and $p_y=p\sin\phi$, $e(>0)$ the elementary charge, and $A(t)=-\int E(t)dt$ the vector potential of the field. We first examine the case where $\mathbf{p}$ is parallel to the field, i.e., $p_y=0$. In this case, Eq. (1) has the following two analytic solutions:

$$\psi(t) = \frac{1}{\sqrt{2}}\exp\left(-i\frac{v_F}{\hbar}\int[p_x+eA(t)]dt\right)\begin{pmatrix}1\\1\end{pmatrix}, \tag{2}$$

$$\psi(t) = \frac{1}{\sqrt{2}}\exp\left(i\frac{v_F}{\hbar}\int[p_x+eA(t)]dt\right)\begin{pmatrix}1\\-1\end{pmatrix}. \tag{3}$$

It can be easily shown that, for each branch, the current $\mathbf{j}=(j_x,j_y)=v_F\psi^\dagger\sigma\psi$ is given by

$$\mathbf{j}=(v_F,0) \quad \text{and} \quad \mathbf{j}=(-v_F,0), \tag{4}$$

respectively. Thus, $\mathbf{j}$ remains constant, i.e., shows no response. This holds true even when the instantaneous kinetic momentum $p_x+eA(t)$ passes by the Dirac point $[p_x+eA(t)=0]$ (Fig. 1). Remarkably, this result indicates that *instantaneous* and *complete* population inversion takes place at the Dirac point irrespective of the frequency, strength, and form of the applied field.

Let us now extend the above discussion to the general case of momentum $\mathbf{p}$. No simple analytic solutions are at hand for $p_y\neq 0$. Equations (2) and (3), however, invite us to make the following ansatz:

$$\psi(t) = c_+(t)\psi_+(t) + c_-(t)\psi_-(t) \tag{5}$$

with

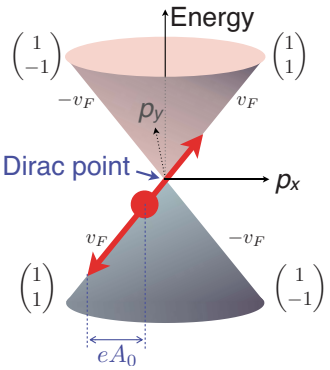

FIG. 1. (Color online) Schematic representation of the dynamics of a single Dirac fermion with $p_y=0$, whose field-free state is marked by a filled circle, under an intense optical-field polarized along the x axis. The bold double-sided arrow corresponds to the variation in the kinetic momentum. A_0 denotes the amplitude of the vector potential. When the electron arrives at the Dirac point, it does not stay in the same band but moves to the other band. The transition is instantaneous and total.

$$\psi_{\pm}(t) = \frac{1}{\sqrt{2}}\exp[\mp i\Omega(t)]\begin{pmatrix} e^{-(i/2)\theta(t)} \\ \pm e^{(i/2)\theta(t)} \end{pmatrix}, \tag{6}$$

where the instantaneous temporal phase $\Omega(t)$ is defined as $\Omega(t)=\frac{v_F}{\hbar}\int\sqrt{[p_x+eA(t)]^2+p_y^2}dt$ and $\theta(t)$ denotes the directional angle of vector $[p_x+eA(t),p_y]$. Substituting Eqs. (5) and (6) into Eq. (1), we obtain, as temporal variation in the expansion coefficients $c_{\pm}(t)$,

$$\dot{c}_{\pm}(t) = \frac{i}{2}\dot{\theta}(t)c_{\mp}(t)e^{\pm 2i\Omega(t)}. \tag{7}$$

Introducing the interband coherence $\rho=c_+c_-^*$ and population difference $n=|c_+|^2-|c_-|^2$, one can rewrite Eq. (7) into a form of extended optical Bloch equations

$$\dot{\rho} = -\frac{i}{2}\dot{\theta}(t)n(t)e^{2i\Omega(t)}, \tag{8}$$

$$\dot{n} = -i\dot{\theta}(t)\rho(t)e^{-2i\Omega(t)} + \text{c.c.} \tag{9}$$

While Eqs. (7)–(9) basically describe interband transitions, they incorporate the field-induced intraband dynamics through $\Omega(t)$ and $\theta(t)$ and are physically more transparent than the TDDE. At the same time, they are totally equivalent with the TDDE involving no approximation. The electron dynamics described by the EOBEs may be experimentally probed, e.g., by time-resolved pump-probe photoemission spectroscopy.[19] Finally, the current is given by

$$j_x = v_F[n\cos\theta + i\sin\theta\{\rho e^{-2i\Omega} - \text{c.c.}\}], \tag{10}$$

$$j_y = v_F[n\sin\theta - i\cos\theta\{\rho e^{-2i\Omega} - \text{c.c.}\}], \tag{11}$$

where the first and second terms correspond to the contribution from the intraband current and interband polarization, respectively. For $p_y=0$, by noting that $\theta(t)$ switches between 0 and π in a stepwise manner at $p_x+eA(t)=0$, one can show that $n(t)$ switches between -1 and 1, and recover Eq. (4).

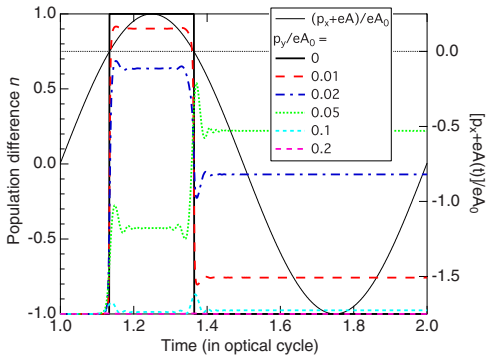

FIG. 2. (Color online) Temporal evolution of the population difference $n(t)$ between the upper and lower states for $p_x/eA_0=-3/4$, $\hbar\omega/v_FeA_0=9.46\times10^{-3}$ and different values of p_y/eA_0 calculated using the EBOEs, except for the case of $p_y=0$, where extracted from Eq. (2). Also, $[p_x+eA(t)]/eA_0$ is plotted in a thin solid line (right axis).

In order to gain insight into how the Dirac fermion behaves when $p_x+eA(t)$ changes its sign, let us consider the first few cycles of a flat-top pulse with a half-cycle ramp on

$$A(t) = \begin{cases} 0 & (t<0) \\ A_0\dfrac{\omega t}{\pi}\sin\omega t & (0\le t<\pi/\omega) \\ A_0\sin\omega t & (\pi/\omega\le t), \end{cases} \tag{12}$$

where $A_0>|p_x|$. We numerically solve the EBOEs for an electron initially in the lower band using the Bulirsch-Stoer method with adaptive stepsize control,[20] for parameters $p_x/eA_0=-3/4$, $\hbar\omega/v_FeA_0=9.46\times10^{-3}$ (corresponding, e.g., to radiation of 1 THz frequency with a field strength of 27.5 kV/cm and $v_Fp_x=-0.33$ eV), and for different values of p_y/eA_0. It should be noted that the coupling element,

$$\dot{\theta}(t) = \frac{p_yeE(t)}{[p_x+eA(t)]^2+p_y^2} \tag{13}$$

is *nonlinear* in $E(t)$ and especially when p_y/eA_0 is small ($\lesssim$0.1), strongly peaks within a narrow time window around $p_x+eA(t)=0$. This leads to a quasisteplike population transfer when $p_x+A(t)$ changes its sign while $n(t)$ is virtually constant otherwise (Fig. 2). The enhanced interband transitions take place even when the gap between the hole and electron states are much larger than the photon energy; the gap is, e.g., $10.6\hbar\omega$ for $p_y/eA_0=0.05$. For $p_y/eA_0\gtrsim0.2$, practically there is no transition.

If we neglected the interband transition, the current j_x would be, by setting $n=-1$ and $\rho=0$ in Eq. (10),

$$j_x = v_F\frac{p_x+eA(t)}{\sqrt{[p_x+eA(t)]^2+p_y^2}}, \tag{14}$$

which would be nonlinear in $A(t)$ when $|eA(t)|>|p_x|,|p_y|$. Thus, one might speculate that graphene would exhibit strongly nonlinear response.[12] However, we have seen above that the interband transition becomes non-negligible exactly for such conditions. Figure 3 compares the evolution of j_x calculated with and without the interband transition. For p_y

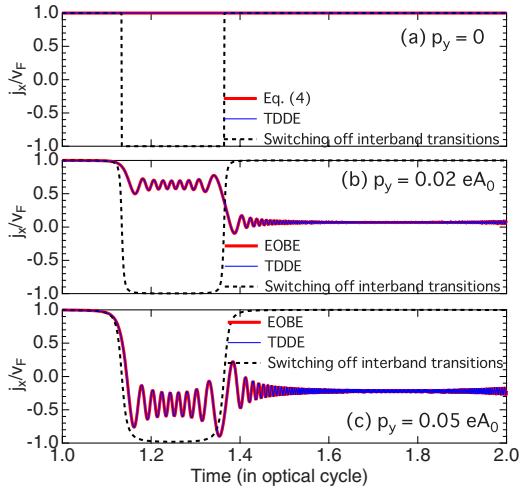

FIG. 3. (Color online) Temporal evolution of the normalized single-electron current $j_x(t)/v_F$ for the same parameters as in Fig. 2 and three different values of p_y/eA_0. Thick solid line: from Eq. (4) for (a) and using the EBOE Eqs. (8)–(10) for (b) and (c), thin solid line: calculated using the TDDE, and dashed line: calculated by switching off the interband transitions, i.e., setting $n=-1$ and $\rho=0$ in Eq. (10) all the time.

$=0$, the interband transition completely cancels the abrupt change expected from purely intraband dynamics. For finite but small values of $|p_y/eA_0|$, the temporal variation in j_x is reduced but still showing nonlinear behavior. In addition, we can see rapid oscillation $\propto e^{-2i\Omega(t)}$ due to interband polarization. In this figure, we also confirm that the results from Eq. (4) and the EBOEs are indisinguishable from those of direct numerical solution of the TDDE.

So far we have focused on the response of a single Dirac fermion. To take into account the Fermi distribution, we solve Eqs. (8) and (9) with initial conditions $n=F(p)-F(-p)$ and $\rho=0$, where $F(p)=\{1+\exp[(v_F p-\mu)/k_B T]\}^{-1}$ is the Fermi-Dirac function with μ, k_B, and T being the chemical potential, Boltzmann constant, and temperature, respectively. Then, the total integrated electric current $\mathbf{J}(t)$ is given by

$$\mathbf{J}(t) = -\frac{g_s g_v e}{(2\pi\hbar)^2}\int \mathbf{j_c}(t)d\mathbf{p}, \tag{15}$$

where $g_s=2$ and $g_v=2$ denote spin- and valley-degeneracy factors, respectively. The carrier current $\mathbf{j}_c$ is to be calculated by replacing n with the carrier occupation $n+1$ in Eqs. (10) and (11), i.e.,

$$j_{c,x} = v_F[(n+1)\cos\theta + i\sin\theta\{\rho e^{-2i\Omega} - \text{c.c.}\}], \tag{16}$$

$$j_{c,y} = v_F[(n+1)\sin\theta - i\cos\theta\{\rho e^{-2i\Omega} - \text{c.c.}\}]. \tag{17}$$

Several remarks are in order. J_y vanishes if the momentum distribution is symmetric with respect to $p_y=0$, which is usually the case. The whole dynamics is invariant under multiplication of quantities of energy dimension, $\hbar\omega$, $v_F p$, $v_F eA$, μ, $k_B T$, and $\hbar/t$ by a common factor. In the weak-field limit, one can derive the universal conductivity $e^2/4\hbar$ from Eqs. (15) and (16).

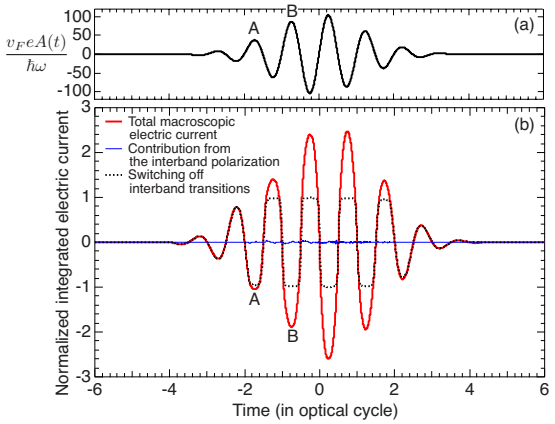

FIG. 4. (Color online) (a) Normalized vector potential $v_F eA(t)/\hbar\omega$ of the incident optical pulse. (b) Temporal evolution of the normalized integrated electric current $J_x/en_s v_F$. Thick solid line: total current calculated with Eqs. (15) and (16), thin solid line: contribution from the interband polarization, and thick dotted line: calculated by switching off the interband transitions, i.e., keeping the initial values of n and $\rho(=0)$ in Eq. (16) all the time. Labels A and B are referred to in Fig. 5.

As an example, let us consider the case where $T=0$ and $\mu=v_F eA_0/5$. The vector potential $A(t)$ is assumed to be a sine pulse with a Gaussian intensity envelope whose full width at half maximum corresponds to two optical cycles and peak amplitude A_0 satisfies $\hbar\omega/v_F eA_0=9.46\times10^{-3}$ as in Figs. 2 and 3 [Fig. 4(a)]. Figure 4(b) displays the normalized current $J_x/en_s v_F$ with $n_s=(g_s g_v \mu^2)/(4\pi\hbar^2 v_F^2)$ being the electron density in the upper cone. If we considered only the intraband dynamics (dotted line), $|J_x/en_s v_F|$ would saturate at unity, which would imply strong nonlinearity.[12] This behavior can be understood by visualizing the carrier occupation distribution at moments A and B marked in Fig. 4 [Figs. 5(a) and 5(b)]. Since the carrier density is fixed and the magnitude of the velocity v_F is independent of momentum, $|J_x/en_s|$ could not exceed v_F. However, in reality, electrons in the lower band transfers to the upper band when they pass near the Dirac point. As a result, we can see substantially more charge carriers at moment B than A [Figs. 5(c) and 5(d)]. This leads to larger electric current at B and its temporal wave form becomes less anharmonic [thick solid line in Fig. 4(b)].

Nonlinear optical response may typically be observed through harmonic generation (frequency multiplication). In Fig. 6 we plot the harmonic intensity spectrum of the coherently emitted radiation $I(\omega)$ given by

$$I(\omega) \propto |\omega\hat{\mathbf{J}}(\omega)|^2. \tag{18}$$

As expected from the previous discussion, the height of the harmonic peaks (thick solid line) is reduced compared with the case of the pure intraband dynamics (thick dotted line). Nevertheless, harmonic generation of up to the 13th order can be seen. It is worth noting that, although the contribution from the interband polarization, i.e., the second term of Eq. (16) is small (thin solid lines in Figs. 4 and 6), the interband dynamics strongly modify the optical response of graphene.

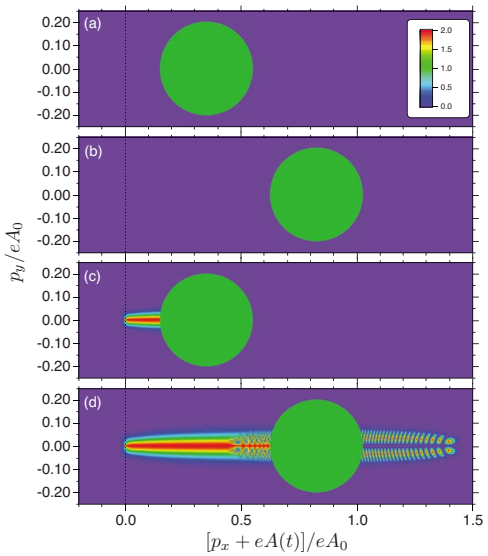

FIG. 5. (Color online) Carrier occupation distribution calculated by switching [(a) and (b)] off and [(c) and (d)] on the interband transitions. (a) and (c) are for the moment labeled as *A* in Fig. 4 and (b) and (d) for *B*.

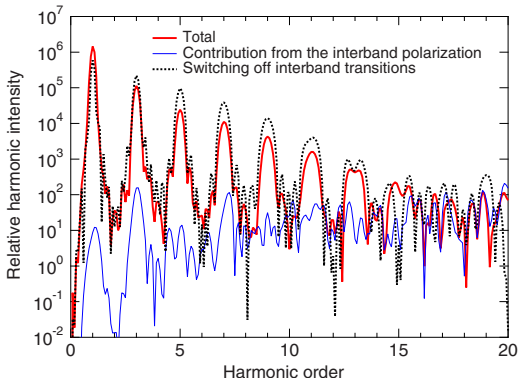

FIG. 6. (Color online) Harmonic intensity spectra for the case of Fig. 4. Thick solid line: total spectrum calculated with Eq. (18), thin solid line: contribution from the interband polarization, and thick dotted line: calculated by switching off the interband transitions.

In conclusion, the time-dependent Dirac equation for massless Dirac fermions can be transformed into a set of extended optical Bloch equations, which are equivalent with the TDDE for a single electron and, at the same time, provide us with clear physical insights, consistently describing the interplay of the intraband and interband temporal dynamics. We have found that, if the component of the electron momentum perpendicular to the field polarization (p_y in this study) is much smaller than eA_0, the interband transition is significantly enhanced when the instantaneous momentum $p_x+eA(t)$ changes its sign. The transition is nonresonant and proceeds within a fraction of optical cycle. Especially for $p_y=0$, instantaneous and complete population transfer takes place at the Dirac point. At the single-electron level, the enhanced interband dynamics relaxes abrupt change in current which would be expected from pure intraband dynamics. After integrating over the Fermi-Dirac distribution, this leads to increase in charge carriers, which reduces nonlinearity in the electric current. Nevertheless, graphene is still expected to show nonlinear optical response such as harmonic generation. It will be straightforward to introduce additional effects such as relaxation and dephasing in the present model (EOBEs), which will be a subject of our next research. Time-domain approaches such as presented here will be increasingly important, in view of recent progress in few-cycle optical pulse technique.[9,10]

This work was supported by the Advanced Photon Science Alliance (APSA) project commissioned by the Ministry of Education, Culture, Sports, Science and Technology (MEXT) of Japan. We thank M. Kuwata-Gonokami for inspiring discussions which led to this study and T. Higuchi, K. Konishi, N. Kanda, and H. Suzuura for fruitful discussions.

*ishiken@atto.t.u-tokyo.ac.jp

[1] K. S. Novoselov, A. K. Geim, S. V. Morozov, D. Jiang, Y. Zhang, S. V. Dubonos, I. V. Grigorieva, and A. A. Firsov, Science **306**, 666 (2004).
[2] A. K. Geim and K. S. Novoselov, Nature Mater. **6**, 183 (2007).
[3] A. K. Geim, Science **324**, 1530 (2009).
[4] K. S. Novoselov, A. K. Geim, S. V. Morozov, D. Jiang, M. I. Katsnelson, I. V. Grigorieva, S. V. Dubonos, and A. A. Firsov, Nature (London) **438**, 197 (2005).
[5] V. P. Gusynin, S. G. Sharapov, and J. P. Carbotte, Phys. Rev. Lett. **96**, 256802 (2006).
[6] A. B. Kuzmenko, E. van Heumen, F. Carbone, and D. van der Marel, Phys. Rev. Lett. **100**, 117401 (2008).
[7] R. R. Nair, P. Blake, A. N. Grigorenko, K. S. Novoselov, T. J. Booth, T. Stauber, N. M. R. Peres, and A. K. Geim, Science **320**, 1308 (2008).
[8] B. Ferguson and X.-C. Zhang, Nature Mater. **1**, 26 (2002).
[9] A. Sell, A. Leitenstorfer, and R. Huber, Opt. Lett. **33**, 2767 (2008).
[10] H. Hirori, M. Nagai, and K. Tanaka, Phys. Rev. B **81**, 081305(R) (2010).
[11] G. Ramakrishnan, R. Chakkittakandy, and P. C. M. Planken, Opt. Express **17**, 16092 (2009).
[12] S. A. Mikhailov and K. Ziegler, J. Phys.: Condens. Matter **20**, 384204 (2008).
[13] A. R. Wright, X. G. Xu, J. C. Cao, and C. Zhang, Appl. Phys. Lett. **95**, 072101 (2009).
[14] E. G. Mishchenko, Phys. Rev. Lett. **103**, 246802 (2009).
[15] H. C. Kao, M. Lewkowicz, and B. Rosenstein, Phys. Rev. B **82**, 035406 (2010).
[16] E. Hendry, P. J. Hale, J. Moger, A. K. Savchenko, and S. A. Mikhailov, Phys. Rev. Lett. **105**, 097401 (2010).
[17] B. Dóra and R. Moessner, Phys. Rev. B **81**, 165431 (2010).
[18] B. Dóra, E. V. Castro, and R. Moessner, Phys. Rev. B **82**, 125441 (2010).
[19] J. K. Freericks, H. R. Krishnamurthy, and Th. Pruschke, Phys. Rev. Lett. **102**, 136401 (2009).
[20] W. H. Press, S. A. Teukolsky, W. T. Vetterling, and B. P. Flannery, *Numerical Recipes in FORTRAN* (Cambridge University Press, Cambridge, 1992).